Published in final edited form as:

Nature. 2017 July 13; 547(7662): 227–231. doi:10.1038/nature22979.

Dystrophin Glycoprotein Complex Sequesters Yap to Inhibit Cardiomyocyte Proliferation

Yuka Morikawa[1], **Todd Heallen**[1], **John Leach**[2], **Yang Xiao**[1], and **James F. Martin**[1,2,3,4]

[1]Cardiomyocyte Renewal Laboratory, Texas Heart Institute, Houston, Texas 77030, USA

[2]Department of Molecular Physiology and Biophysics, Baylor College of Medicine, Houston, Texas 77030, USA

[3]Program in Developmental Biology, Baylor College of Medicine, Houston, Texas 77030, USA

[4]Cardiovascular Research Institute, Baylor College of Medicine, Houston, Texas 77030, USA

Summary

The regenerative capacity of the adult mammalian heart is limited because of the reduced ability of cardiomyocytes (CMs) to progress through mitosis[1]. The regenerative capacity of endogenous CMs exists at birth but is lost postnatally, with subsequent organ growth occurring through CM hypertrophy[2,3]. The Hippo pathway, a conserved kinase cascade, inhibits CM proliferation in the developing heart to control heart size and in the adult heart to prevent regeneration[4,5]. The dystrophin glycoprotein complex (DGC), a multicomponent transmembrane complex linking the actin cytoskeleton to extracellular matrix, is essential for CM homeostasis. DGC deficiency in humans results in muscular dystrophy, including lethal Duchenne muscular dystrophy (DMD). We found that the DGC component dystroglycan 1 (DAG1) directly binds to Hippo pathway effector Yap to inhibit CM proliferation. The Yap-DAG1 interaction was enhanced by Hippo-induced Yap phosphorylation, revealing a connection between Hippo pathway function and the DGC. After injury, Hippo-deficient postnatal hearts maintained organ size control by repairing the defect with correct dimensions, whereas postnatal hearts doubly deficient for Hippo and the DGC showed CM overproliferation at the injury site. In mature *Mdx* mouse hearts—a model of DMD—Hippo deficiency protected against overload-induced heart failure.

Previous work revealed that DGC components are Yap targets[6]. To explore the connection between the Hippo pathway and DGC function, we conditionally deleted the gene encoding

Correspondence and requests for materials should be addressed to jfmartin@bcm.edu.

Online Content: Methods, along with any additional Extended Data display items and Source Data, are available in the online version of the paper at www.nature.com/nature; references unique to these sections appear only in the online paper.

Author Contributions: J.F.M. and Y.M. conceived the project and designed the experiments. Y.M. performed experiments and analyzed data. T.H. performed immunoprecipitation, protein binding assay, and Western blotting. J.L. performed cardiac function analysis and experiments on AAV9 viral studies. Y.X. performed several immunohistochemical studies. J.F.M., Y.M., and J.L. performed statistical analyses. J.F.M supervised the project and analyzed data. Y.M. and J.F.M. wrote the manuscript. All authors edited and approved the manuscript.

Competing Financial Interests: The authors declare no competing financial interests.

the Hippo pathway component Salvador (*Salv*) in myocardium in an *Mdx* (dystrophin loss of function) background[4,7]. Neonatal cardiac apex resections were performed at nonregenerative postnatal (P) day 8, and resected hearts collected at P29 revealed that control and *Mdx* hearts failed to regenerate (Fig. 1a, b, e, f, h), whereas *Salv* conditional knockout (CKO) hearts regenerated efficiently (Fig. 1c, e, g). Remarkably, *Salv*; *Mdx* double knockout (DKO) hearts regenerated with excessive myocardial growth at the resection site, often with a completely formed secondary cardiac apex (Fig. 1d, e, i, j). Both *Salv* CKO and *Salv*;*Mdx* DKO resected hearts had reduced scarring, indicating efficient cardiac repair (Fig. 1c, d, e).

Immunofluorescence studies in *Salv*;*Mdx* DKO secondary apex CMs 21 days after resection revealed that CM length was unchanged when compared to that in other groups (Extended Data Fig. 1a-m). In the *Salv* CKO, regenerating CMs displayed an organized alignment when measured against the resection plane[8]; however, *Salv*;*Mdx* DKO CMs had a broad range of orientations and appeared disorganized (Extended Data Fig. 1n, o), indicating that CM outgrowth in the *Salv*;*Mdx* DKO secondary apex was uncoordinated. This overgrowth phenotype suggests that the Hippo pathway and DGC cooperatively limit tissue growth after injury and that DGC function is required for the normal three-dimensional organization of regenerating CMs.

We previously discovered cellular protrusions in regenerating *Salv* CKO border zone CMs[6]. In regenerative stage hearts, when Hippo activity is low, protrusion formation promoted regeneration; however *Mdx* CMs failed to make protrusions and regenerate, indicating the requirement for dystrophin[6]. We determined whether protrusion formation could be rescued after injury at the non-regenerative stage in *Salv*;*Mdx* DKO adult hearts. Whereas *Salv* CKO border zone CMs formed protrusions, *Salv*;*Mdx* DKO CMs failed to make protrusions (Extended Data Fig. 2a-e). Similarly, vinculin expression was elevated in *Salv* CKO border zone CMs but not in those of other groups (Extended Data Fig. 2f-m). *In vitro* migration studies also revealed that dystrophin deficiency in *Salv*;*Mdx* DKO hearts suppressed the migratory phenotype of *Salv* CKO CMs (Extended Data Fig. 2n-r), suggesting that the disorganized morphology of regenerated CMs in *Salv*;*Mdx* DKO hearts was due to lack of protrusion formation.

DNA synthesis and expression of the mitosis and cytokinesis marker aurora kinase B (Aurkb) were increased in injured *Salv*;*Mdx* DKO CMs compared to injured control CMs (Fig. 1k, l), indicating enhanced myocardial proliferation in *Salv*;*Mdx* DKO hearts. After apex resection, *Salv* CKO and *Salv*;*Mdx* DKO CMs showed increased cytokinesis compared to control CMs (Fig. 1l-p). Similar to DNA synthesis, cytokinesis was increased in *Salv*;*Mdx* DKO CMs compared to *Salv* CKO CMs. These results indicate that the Hippo pathway and DGC cooperatively inhibit CM cell cycle progression.

To investigate whether the DGC regulates Yap by altering its subcellular localization after injury, we examined Yap localization in border zone CMs after apex resection. The number of CMs with nuclear Yap was low in control and *Mdx* hearts (Fig. 2a, b, e, f, i) but was elevated in *Salv* CKO hearts (Fig. 2c, g, i), as reported previously[6]. In *Salv*;*Mdx* DKO hearts, Yap was localized in the nucleus of most CMs (Fig. 2d, h, i). Furthermore, the

expression of Yap targets Ccne2 and Talin was upregulated in *Salv* CKO and *Salv*;*Mdx* DKO CMs (Fig. 2j-a′). These results suggest that the Hippo pathway and DGC cooperatively inhibit Yap nuclear localization to prevent Yap transcriptional activity.

Dilated cardiomyopathy (DCM) with heart failure and myocardial fibrosis develops in DMD patients and approximately 10% of female carriers[9]. Mice were challenged with transverse aortic constriction (TAC)—an overload model of DCM with fibrosis, CM loss, and heart failure[10] (Extended Data Fig. 3a-g). Two weeks after TAC, *Salv* CKO and *Salv*;*Mdx* DKO CMs were smaller than control and *Mdx* CMs (Extended Data Fig. 3g). *Mdx* hearts showed DCM with decreased heart function and increased fibrosis, indicating that *Mdx* hearts were prone to DCM (Fig. 3a-k; Extended Data Fig. 4a-e)[11]. In contrast, *Salv*;*Mdx* DKO hearts showed less severe dilation, less replacement fibrosis, and maintained cardiac function equivalent to that of control and *Salv* CKO hearts (Fig. 3a-k; Extended Data Fig. 4a-e). *Mdx* mice challenged with TAC undergo CM loss[11]. CM number was higher in *Salv*;*Mdx* DKO hearts than in *Mdx* hearts (Fig. 3l). *Salv*;*Mdx* DKO hearts showed increased numbers of EdU-positive diploid (2N) CM nuclei that were enriched in peri-fibrotic areas and aurkb expressing CM, indicating increased proliferation (Fig. 3m, n, o, Extended Data Fig. 5a-z, 6a-d). More CMs had nuclear Yap in *Salv* CKO and *Salv*;*Mdx* DKO hearts than in *Mdx* hearts (Fig. 3p; Extended Data Fig. 6e-l). The higher number of CMs in *Salv*;*Mdx* DKO hearts than in *Mdx* hearts was partly because of reduced apoptosis, particularly one week after TAC (Fig. 3q, Extended Data Fig. 6m-t). Furthermore, cytoplasmic phosphorylated (P)-Yap levels were lower in *Salv* CKO and *Salv*;*Mdx* DKO CMs than in control and *Mdx* CMs (Extended Data Fig. 7a-i). Unlike in the resection model, vinculin expression was comparable among the 4 genotypes (Extended Data Fig. 7j-q). These results suggest that suppression of *Mdx* cardiomyopathy by deleting *Salv* is due to increased CM proliferation and, immediately after TAC, to reduced apoptosis.

To investigate Hippo deficiency in *Mdx* C57BL/10J mice using gene therapy, we performed TAC and injected an adeno-associated virus 9 (AAV9) encoding *Salv*sh RNA or a control virus (Fig. 3r-v; Extended Data Fig. 8a-e)[12]. Compared to the control knockdown, *Salv* knockdown preserved cardiac function, increased nuclear Yap and Yap target gene expression, and reduced fibrosis in TAC-challenged *Mdx* C57BL/10J hearts (Fig. 3r-v; Extended Data Fig. 8f-k). The mRNA levels of Yap target genes encoding proteins that regulate cell proliferation increased to a greater extent than did those of genes encoding cytoskeletal components (Fig. 3u), perhaps reflecting differences in sensitivity to Yap.

We determined whether DGC complex components directly interact with Yap in control and *Mdx* P12 heart extracts. DAG1 contains a PPxY motif that binds WW domain–containing proteins, such as Yap and dystrophin[13]. Yap pulldowns revealed that Yap associated with DGC components Sgcδ and DAG1 in control but not *Mdx* extracts, whereas the interaction between Yap and Lats2, as well as an interaction between Yap and α-catenin was detected in both control and *Mdx* extracts (Fig. 4a). DAG1 pulldowns revealed that DAG1 associated with Sgcδ and Yap in control but not *Mdx* extracts (Fig. 4b). Lats2 did not associate with DAG1, suggesting that Hippo pathway components did not form a complex with the DGC. Using the C2C12 myoblast cell line, we found that Yap interacted with DGC components

but that the interaction was disrupted when the gene encoding dystrophin (*Dmd*) was knocked down (Extended Data Fig. 9a, b).

P-Yap was present in the DGC (Fig. 4b; Extended Data Fig. 9d), suggesting that Yap phosphorylation by Lats kinase promotes the interaction between Yap and the DGC. To test this, we examined the interaction between Yap and the DGC in cardiac extracts from transgenic mice expressing Flag-tagged Yap—Yap5SA—that is impervious to the Hippo kinase cascade in adult CMs[14]. Yap5SA did not interact with DGC components or Lats2 but did interact with α-catenin (Fig. 4c, d). In Yap5SA-transfected C2C12 cells, neither DGC components nor Lats2 interacted with Yap5SA (Extended Data Fig. 9c, d). DAG1 interacted with endogenous Yap but not Yap5SA (Fig. 4d; Extended Data Fig. 9d). Similar to what we observed in the heart, Lats2 and DAG1 did not interact in C2C12 cells (Extended Data Fig. 9d).

C2C12 cell fractionation experiments revealed that, in control cells, Yap was localized in the plasma membrane, cytoplasm, and nuclear fractions (Fig 4e-h). Compared to control cells, *Salv* knockdown C2C12 cells and *Salv;Dmd* knockdown C2C12 cells had decreased Yap localization in the plasma membrane and cytoplasmic fractions and increased Yap localization in the nuclear fraction (Fig. 4e-h). In contrast to CMs, *Dmd* knockdown C2C12 cells had more nuclear Yap. A difference between C2C12 cells and CMs is the presence of the intercalated disc (ICD) in mature CMs. Because Yap binds α-catenin that localizes to the ICD in CMs, Yap binding to the ICD may compensate for DGC deficiency in CMs (Fig. 4a, c)[15]. Super resolution microscopy revealed that Yap colocalized with DAG1 in the plasma membrane in control but not *Mdx* CMs (Fig. 4i-l). However, Yap colocalized in the ICD with connexin 43 (Cx43) in both control and *Mdx* CMs (Fig. 4m-p). In addition, experiments with purified GST fusion proteins revealed that Yap directly bound DAG1 through the DAG1 PPxY motif but did not directly interact with Sgcδ (Fig. 4q). Therefore, Yap phosphorylation is not required for DAG1 binding *in vitro*. Collectively, these data suggest that Hippo phosphorylation of Yap promotes the Yap-DGC complex formation *in vivo*.

The DGC is a node for mechanical signaling. Mechanical signaling regulates Yap subcellular localization, but the mechanism is poorly understood[16]. Our data reveal that the DGC sequesters P-Yap, perhaps to prevent the action of activating phosphatases, as a mechanism to regulate CM proliferation in the postnatal and adult heart (Extended Data Fig. 10). Our findings suggest exquisite coordination of extracellular and mechanical signaling with nuclear events in the context of a mechanically stressed CM. The Hippo-Yap-DGC negative regulatory loop is dysfunctional in the stressed CM, preventing an adequate proliferative response. Our findings also indicate that Hippo signaling is maladaptive in DMD cardiomyopathy and raise the possibility that Hippo deficiency, in combination with other approaches such as gene editing, can be used to treat muscular dystrophy[17-19].

Methods

Mice

Control (*Mhy6-Cre*^{ert}; mTmG), *Mdx* (*Mdx*;*Mhy6-Cre*^{er};mTmG), *Salv* CKO (*Salv*$^{fx/fx}$;*Mhy6-Cre*^{ert};mTmG), and *Salv*;*Mdx* DKO (*Salv*$^{fx/fx}$;*Mdx*;*Mhy6-Cre*^{ert};mTmG) mice were used for genetic studies. For studies involving AAV9 infection, C57-BL/10ScSn-Dmd^{mdx}/J mice (The Jackson Laboratory, Bar Harbor, ME, USA) were used. Because the allele encoding dystrophin is X-linked, only male mice were used in this study. The gain-of-function transgenic Yap 5SA mouse line was created by injecting mice with the CAG-loxP-eGFP-Stop-loxP-Flag YAP2 5SA-IRES-βGal plasmid[12]. The sequence of Flag-YAP2 5SA was obtained from the pCMV-Flag YAP2 5SA plasmid (a gift from Kun-Liang Guan (UCSD), Addgeneplasmid #27371). *Mhy6-Cre*^{ert} mice were crossed with hemizygous Yap5SA mice. To induce the expression of Yap5SA in CMs, tamoxifen (150 mg) was injected daily for 4 days into 6-week-old Yap5SA;*Mhy6-Cre*^{ert} mice.

For each experimental group, we studied a minimum of 3 mice that were randomized by using block randomization. We estimated sample sizes based on our pilot studies. Mice were used for these studies because they are amenable to genetic manipulation and can be made into models of human diseases. All animal protocols and procedures were approved by the Institutional Animal Care and Use Committee (IACUC) of Baylor College of Medicine in Houston, Texas. For all surgeries and echocardiographic studies, researchers were blinded from mouse genotypes.

Apex resection

Resection of the heart apex or sham surgery was performed at P8 in mice, as previously described[4]. Tamoxifen (50 mg) was injected daily from P7 to P10. Hearts were collected at 4 and 21 days after resection. For data in Figure 1, Sham or apex resection was performed in nonregenerative-stage hearts (postnatal day 8) of control, *Mdx*, *Salv* conditional knockout (CKO), and *Salv*;*Mdx* double knockout (DKO) mice. All mice carried the *Myh6-Cre*^{ERT};*mTmG* allele, and tamoxifen was administered daily from P7 to P10.

Transverse aortic constriction (TAC)

Mice were challenged with TAC because *Mdx* mice have a mild phenotype and develop cardiomyopathy after aging to approximately 15 months[20]. On the day of surgery and 1 day after surgery, 9- to 10-week-old mice were injected with tamoxifen (150 mg). The thoracic aorta between the carotid arteries was constricted by using 6-0 silk thread between the carotid arteries. Mice that did not survive overnight from the surgery were excluded. Echocardiographic analysis was performed on the day before surgery and 2 weeks after the surgery. For the studies involving AAV9, echocardiography was performed prior to surgery and 2, 8, and 11 weeks after surgery. TAC and sham surgeries were performed in C57BL/10J *Mdx* mice. For knockdown studies, AAV-GFP (green fluorescent protein) or AAV-*Salv* virus was administered at the time of surgery. In Figure 3 r, s, *Mdx* sham groups prior to viral injection at week 0 were collapsed into one group (Sham pre-treatment).

Cardiac function analysis

Echocardiography was performed in the Baylor College of Medicine Mouse Phenotyping Core. Transthoracic echocardiography was performed by using the VisualSonics Vevo 2100 system equipped with a 40Mhz 550s probe. Mice were anesthetized with 2% isoflurane inhalation (driven by 2 L/min oxygen) and placed on a heated platform (37°C) with integrated physiologic monitoring capabilities. Two-dimensional B-mode imaging was used to capture the long-axis projection with guided M-Mode images, and a PW Doppler pulse wave was recorded for associated echocardiographic measurements. The average reading for each echocardiographic parameter was recorded from at least 3 distinct frames from each mouse.

AAV9 targeting *Salv*

The parental vector pENN.AAV.cTNT, p1967-Q was obtained from the University of Pennsylvania Vector Core. A triple miR30–flanked shRNA directed at *Salv* was cloned downstream of a green fluorescent protein (GFP) reporter. The subsequent construct was packed into AAV9 by the IDDRC Neuroconnectivity Core at Baylor College of Medicine. Mice were administered a single retro-orbital injection of virus with a total of 1×10^{12} viral genomes delivered, and TAC or sham surgery was performed. Hearts were collected 13 weeks after the surgery.

Histologic analysis

For apex resection studies, hearts were collected 3 weeks after the surgery. For TAC genetic studies, hearts were collected 2 weeks after surgery. Hearts were fixed in 10% formalin, embedded into paraffin, and sectioned for further analysis. For AAV9 studies, hearts were collected 11 weeks after surgery; hearts were then frozen and sectioned for further analysis.

Trichrome staining was performed to determine the degree of heart injury or fibrosis. Fibrotic scarring stained blue, and scar size was measured by using ImageJ software. The size of the extra apex was determined by drawing a line at the site of resection and measuring the area outside of the line by using ImageJ software.

Immunohistochemistry

Paraffin-embedded and frozen tissues were used for immunohistochemical analysis. For paraffin-embedded sections, samples were deparaffinized and rehydrated, treated with 3% H_2O_2 in EtOH, treated with antigen retrieval solution (Vector Laboratories, Inc., Burlingame, CA, USA), blocked with 10% donkey serum in phosphate-buffered saline (PBS), and then incubated with primary antibodies. For frozen sections, samples were fixed with acetone, treated with 0.3% H_2O_2 in PBS, treated with 0.1 M ammonium chloride, blocked with 10% donkey serum in PBS, and then incubated with primary antibodies. Primary antibodies were detected with fluorescently labeled secondary antibodies. Primary antibodies used in this study were as follows: mouse anti-cardiac troponin T (Thermo Fisher Scientific Inc., Waltham, MA, USA), mouse anti-vinculin (Thermo Fisher), mouse anti-ß-dystroglycan (Santa Cruz Biotechnology, Inc., Dallas, TX, USA), mouse anti-Salvador (Santa Cruz), rabbit anti-Yap1 (Novus Biologicals, LLC, Littleton, CO, USA), rabbit anti-phospho Yap (Cell Signaling Technology, Inc., Danvers, MA, USA), rabbit anti–aurora

kinase B (Abcam, Cambridge, UK), rabbit anti–sarcomeric actinin (Abcam), rabbit anti-CCNE2 (Abcam), mouse anti-Talin (Sigma-Aldrich Co. LLC., St. Louis, MO, USA), mouse anti-connexin 43 (Santa Cruz), rabbit anti-active caspase 3 (Abcam), and rabbit anti-phosphohistone H3 (PHH3) (Abcam). Secondary antibodies used in this study were as follows: Alexa-546– or Alexa-647– conjugated anti-rabbit (Thermo Fisher), biotin-conjugated anti-mouse (Vector), and Alexa-488–conjugated streptavidin (Thermo Fisher). Immunostained samples were analyzed by using a Leica TCS SP5 confocal microscope. Images were processed by using Leica LAS AF software. Images from 3 different sections were documented for each sample.

For the quantification of CMs positive for AurkB, Yap, active caspase 3, and CCNE2, positive-staining CMs were quantified manually by using ImageJ software. The observer was blinded to genotypes. The quantification of CMs positive for Talin, Salv, and P-Yap was performed by measuring pixel intensity in the CM cytoplasm. When images were captured, intensity was normalized to the level of staining in fibroblasts.

Deconvolution epifluorescence microscopy was performed in the Baylor College of Medicine Integrated Microscopy Core by using an OMX-BLAZE 3D structured illumination microscope (GE Healthcare Life Systems, Pittsburgh, PA, USA). Images were acquired with an Olympus PlanApo 60×/1.42 objective, in z-stacks with 0.125 μm spacing covering most of the tissue thickness. Images were deconvolved by using a conservative algorithm. The maximum intensity projected and histogram were adjusted by using SoftWorX 6.5.2. Three-dimensional volumes were also generated with the same software.

To quantify the number and size of CMs, cells were delineated by using wheat germ agglutinin (WGA) conjugated with Alexa 647 (Thermo Fisher). Tissues were costained with anti-cardiac troponin T to label CMs, and images were captured under a fluorescent microscope. The number and size of CMs were quantified manually by using ImageJ software. The observer was blinded to genotypes.

In CMs stained for cTNT, sarcomere length was measured manually by using ImageJ software. The observer was blinded to genotypes. CM orientation angles were measured manually by using ImageJ and were referenced to the plane of resection.

EdU incorporation analysis

For EdU incorporation studies on P8 resection models, 0.25 mg of EdU (5-ethynly-2-deoxyurindine) was injected into apex-resected animals at 4 hr before harvest on 4 days after resection. EdU incorporation was analyzed in paraffin-embedded tissues by using a Click-it EdU Imaging Kit (Thermo Fisher), followed by staining for cTNT and WGA. The number of EdU-positive nuclei was counted manually by using ImageJ software. The observer was blinded to genotypes.

For EdU incorporation studies on adult TAC models, 100 μg/g mouse of EdU was injected daily, starting at 2 days after surgery until 1 day before harvest. Hearts were harvested and nuclei were isolated for flow analysis according to previously described [21,22]. In brief, nuclei were stained with PCM1 antibody (Sigma-Aldrich) and for EdU using Click-it EdU Flow

Cytometry Assay Kit (Thermo Fisher). Analysis of nuclei was performed at Texas Heart Institute Flow Cytometry Core Facility using BD FACSAria (BD Biosciences). For EdU performed on sections, peri-fibrotic area was defined as within 350μm from the replacement fibrosis that was only observed in *Mdx* and *Salv;Mdx* DKO hearts.

Collagen gel assay

We used the collagen gel assay to analyze P10 hearts, as previously described[6]. Gels were stained for cTNT and with DAPI to detect the migration of CMs to the bottom gel.

Quantitative real-time (RT)-PCR

Total RNA was extracted from frozen heart tissue by using the RNAeasy Micro kit (Qiagen, Hilden, Germany). Quantitative RT-PCR was performed as previously described[6] by using the StepOnePlus Real-Time PCR System (LifeTechnologies).

Immunoprecipitation and Western blotting

Immunoprecipitation and Western blotting were performed as previously described,[5] with the following minor modifications. Hearts were treated with modified radioimmunoprecipitation assay (RIPA) lysis buffer (50 mMTris-HCl, pH 7.4, 50 mMNaCl, 1 mM EDTA, 0.2% sodium deoxycholate, 0.05% sodium dodecyl sulfate [SDS], 0.2% Triton X-100, 0.5% NP-40) supplemented with complete protease and phosphatase inhibitors (The Roche Group, Basel, Switzerland).

Protein concentration was determined by using a Qubit Protein Assay Kit on a Qubit 3.0 Fluorometer (Thermo Fisher). Primary antibodies used for immunoprecipitation were as follows: anti-Yap1 (5μg; Novus) and anti-DAG1 (3μg; Abcam). Anti-Flag M2 affinity gel (Sigma-Aldrich) was used for Flag pulldown assays. Primary antibodies used for immunoblotting were as follows: anti-Yap1 (1:1000 dilution; Novus), anti–phospho-Yap (Ser127) (1:1000; Cell Signaling), anti-LATS2 (1:500 dilution; Bethyl Laboratories), anti-SGCD (1:500 dilution; Santa Cruz), anti-DAG1 (1:500 dilution; Abcam), anti–α-catenin (1:50000 dilution; Abcam), and anti-Flag (1:1000 dilution; Sigma-Aldrich).

For the Yap5SA experiments, expression of Yap5SA in CMs was induced by tamoxifen injection starting 5 days before harvest for 4 consecutive days. For experiments performed in C2C12 cells, subcellular protein lysate fractions were collected from differentiated C2C12 cells after siRNA-mediated knockdown of *Salv* and/or the gene encoding dystrophin (*Dmd*).

Cell Culture

C2C12 cells (ATCC CRL-1772) were cultured in Dulbecco's modified Eagle medium (D-MEM; Thermo Fisher) supplemented with 20% fetal bovine serum (HyClone, GE Healthcare Life Systems) and 1× penicillin/streptomycin (Thermo Fisher). Cells were tested for mycoplasma by using a Myco Probe mycoplasma detection kit (R&D Systems). To induce differentiation, confluent cells were treated with differentiation media containing D-MEM supplemented with 2% horse serum (Thermo Fisher) and 1× penicillin/streptomycin.

For immunoprecipitation studies, cells were differentiated for 7 days. For *Dmd* knockdown studies, Lipofectamine RNAiMax (Thermo Fisher) was used to transfect siRNA into differentiated cells 2 days before harvest. Yap5SA (pCMV-Flag Yap2) or GFP plasmid was transfected into C2C12 cells by using Lipofectamine 3000 (Thermo Fisher) one day before the differentiation treatment was started. For subcellular fractionation, cells were differentiated for 3 days and treated with siRNA at day 1 of differentiation for 48 hours before harvest. Nuclear, cytoplasmic, and plasma membrane fractions of cellular extracts were prepared by using a subcellular protein fractionation kit for tissues (Thermo Fisher) according to the manufacturer's instructions.

Recombinant GST-fusion proteins and binding assays

The GST-YAP1 plasmid was a kind gift from Stefano Piccolo (University of Padova, Italy). GST-DAG1 (ß-dystroglycan domain, amino acids 652-893 of DAG1) and GST-SGCD (full-length, amino acids 1-289) were created by Gibson Assembly DNA cloning (NEB, Ipswich, MA, USA) by using synthesized gBlocks gene fragments (IDT) for in-frame fusion with the GST moiety of pGEX-4T-2. To generate the DAG1ΔPPxY mutant, we deleted the C-terminal PPxY domain (amino acids 887-890) of DAG1 by using PCR-based site-directed mutagenesis with the NEBaseChanger tool and the Q5 Site-Directed Mutagenesis kit (NEB). All constructs were confirmed by DNA sequencing. Recombinant GST proteins were expressed in the *E. coli* strain BL21 (DE3) (ThermoFisher) by induction with 1 mM isopropyl β-D-1-thiogalactopyranoside (IPTG) for 24 hours. Bacterial pellets were lysed in GST lysis buffer (1× PBS, 20 mM HEPES, 1 mM EGTA, 0.2% Triton X-100) supplemented with cOmplete, Mini, EDTA-free Protease Inhibitor and PhosSTOP phosphatase inhibitor cocktails (Sigma-Aldrich). After brief sonication of the lysates, 50% glutathione-S-transferase resin (GE Healthcare) was added, and samples were rocked at 4°C for 4 hours for the affinity purification of GST-tagged proteins.

For *in vitro* binding assays, purified GST proteins (500 mM) were treated with thrombin protease (GE Healthcare) to remove the GST tag. Cleaved proteins were then mixed with GST-YAP1 or GST-DMD bound to glutathione beads and were rocked over ice for 3 hours. Beads were washed three times by rocking in PBS+20 mM HEPES with 0.2% Triton X-100 at 4°C for 5 minutes and were pelleted. Samples were separated by using SDS-polyacrylamide gel electrophoresis, transferred to PVDF membranes, and analyzed via Western blotting.

Estimation of Cardiomyocyte Numbers on Sections

For each section, total number of CMs was estimated from the number of CMs in 0.1 mm^2 area multiplied by the total area.

Statistical Analysis

The *n* number for each experiments and analysis used in each panel are stated in each section of figure legends. All bar graphs except for Extended Data Figure 1o represent mean ±s.e.m.

Data availability

The data that support the findings of this study are available from the corresponding author upon reasonable request.

Extended Data

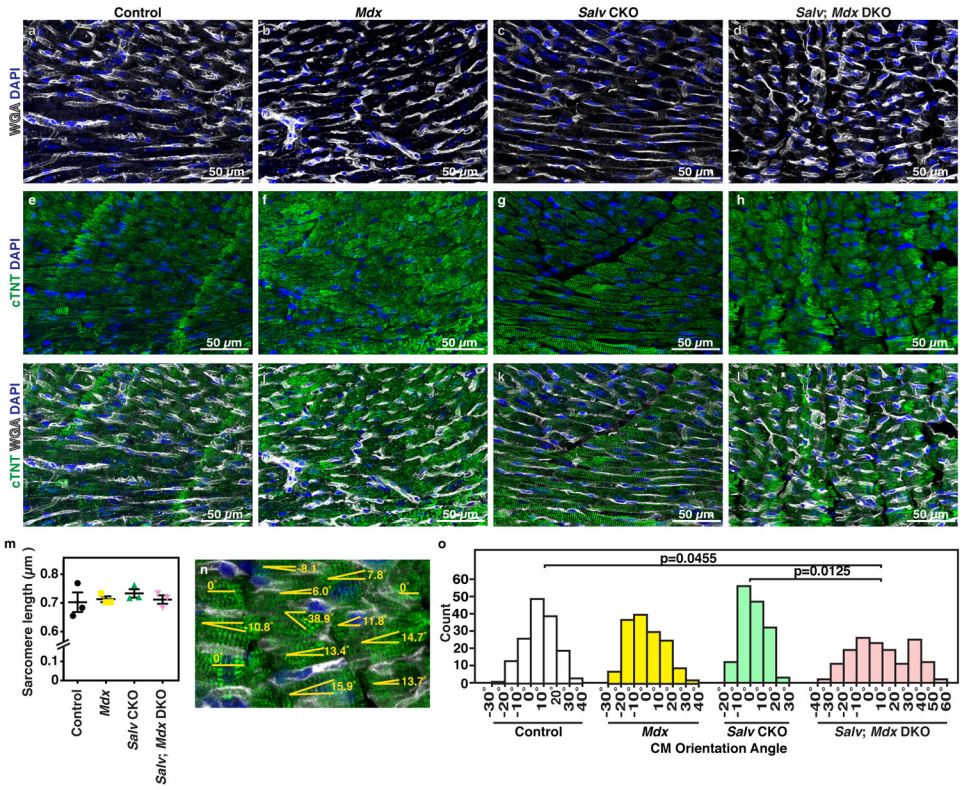

Extended Data Figure 1. Cardiomyocyte alignment after apex resection in P8 mouse hearts

a-o, Hearts were collected 21 days after apex resection was performed in P8 mice. Hearts of control (**a, e, i**), *Mdx* (**b, f, j**), *Salv* conditional knockout (CKO) (**c, g, k**), and *Salv*;*Mdx* double knockout (DKO, **d, h, l**) mice were stained for cardiac troponin T (cTNT) and wheat germ agglutinin (WGA) for CMs and cell membranes, respectively. For control and *Mdx* hearts, the apex regions above the scar are shown. For *Salv* CKO and *Salv;Mdx* DKO hearts, the apex regions that regenerated are shown. **m**, Sarcomere length in each CM was measured. Groups were compared by using one-way analysis of variance (n=3 for each genotype). No statistically significant difference was observed between samples. **n, o,** CM orientation in either the border zone or repaired area. In panel n, a representative image shows how the orientation angles of CMs were measured. Angles referenced to the plane of resection were measured for each CM. A total of 50 CMs were measured for each sample. **o**, Histograms showing the distribution of CM orientation angles for each genotype (n=3 for each genotype; 150 CMs total were analyzed for each genotype). Variance between genotype groups was compared by using an F-test.

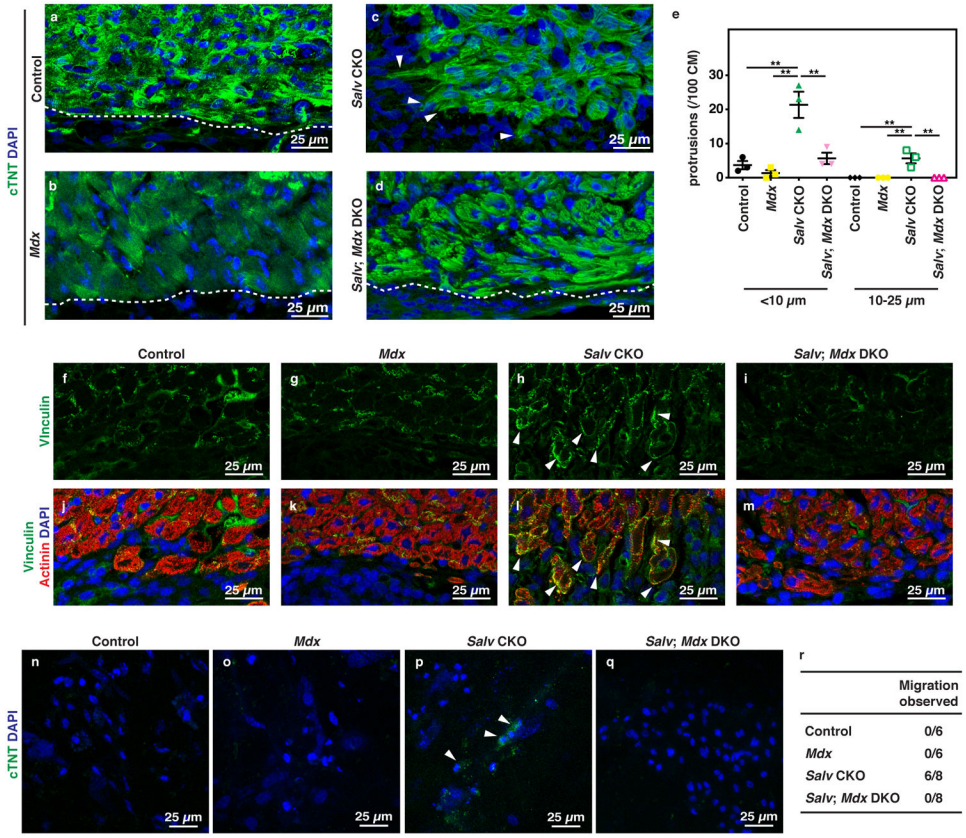

Extended Data Figure 2. Protrusion formation in border zone cardiomyocytes and migration of postnatal cardiomyocytes after apex resection in mice

a-e, Apex resection was performed in P8 hearts of control (**a**), *Mdx* (**b**), *Salv* conditional knockout (CKO) (**c**), and *Salv*;*Mdx* double knockout (DKO, **d**) mice, and hearts were collected 4 days after resection. CMs were stained for cardiac troponin T (cTNT), and images were documented of the tissue around border zone CMs. Dotted lines show plane of resection. Arrowheads show CM protrusions. **e**, Quantification of CM protrusions (n=3 for each genotype). CMs adjacent to the scar were analyzed for length and number of protrusions 4 days after resection. One hundred CMs from each heart were analyzed. Groups were compared by using analysis of variance (ANOVA) with Bonferroni's multiple comparison test for pairwise comparisons. **p<0.01. CM, cardiomyocyte. **f-m**, Immunostaining for vinculin to visualize cytoskeletal rearrangement in border zone CMs of control (**f, j**), *Mdx* (**g, k**), *Salv* CKO (**h, l**), and *Salv*;*Mdx* DKO (**i, m**) mouse hearts. CMs were labeled with anti-sarcomeric actinin. Arrowheads indicate where the upregulation of vinculin is visible in *Salv* CKO border zone CMs. **n-r**, Collagen gel assay results for P10 hearts collected from control (**n**), *Mdx* (**o**), *Salv* CKO (**p**), and *Salv*;*Mdx* DKO mice (**q**). Gel was stained with DAPI and for cTNT. **r**, Quantification of hearts in which migration was observed. Groups were compared by using the Fisher's exact test. Control vs *Salv* CKO, p=0.0097; *Mdx* vs *Salv* CKO, p=0.0097; *Salv* CKO vs *Salv*;*Mdx* DKO, p=0.007.

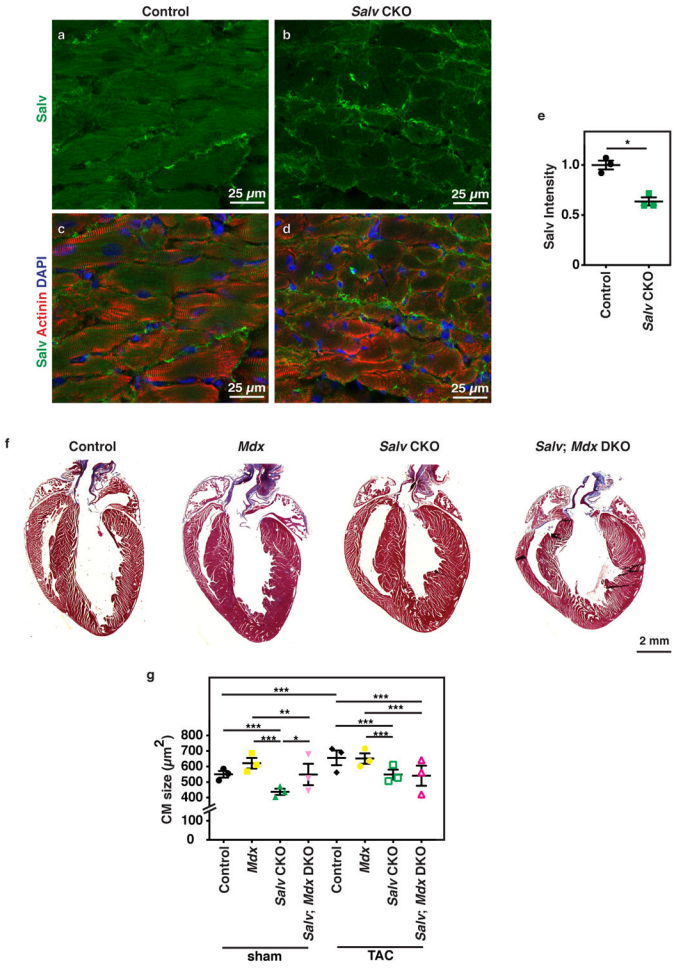

Extended Data Figure 3. Characterization of mouse hearts after transverse aortic constriction surgery

a-e, Knockout efficiency in *Salv* conditional knockout (CKO) mice. Immunohistochemical analysis of Salv was performed in control (**a, c**) and *Salv* CKO (**b, d**) mouse hearts 2 weeks after transverse aortic constriction (TAC) surgery. CMs were labeled with anti-sarcomeric actinin. **e**, Quantification of Salv intensity (n=3 for each treatment) measured according to pixel intensity. Groups were compared by using the Mann-Whitney U test (n=3 for each treatment). *p<0.05. **f-g** Histology and cell size after TAC surgery. **f,** Representative images showing trichrome staining of hearts 2 weeks after TAC surgery in control *Mdx*, *Salv* CKO, and *Salv*;*Mdx* double knockout (DKO) mice. **g**, CM size 2 weeks after sham or TAC surgery. Cell size was measured in wheat germ agglutinin (WGA)-stained sections by using ImageJ software. Groups were compared by using analysis of variance (ANOVA) with Bonferroni's post-hoc test for pairwise comparisons (n=3 each). *p<0.05, **p<0.01, ***p<0.001.

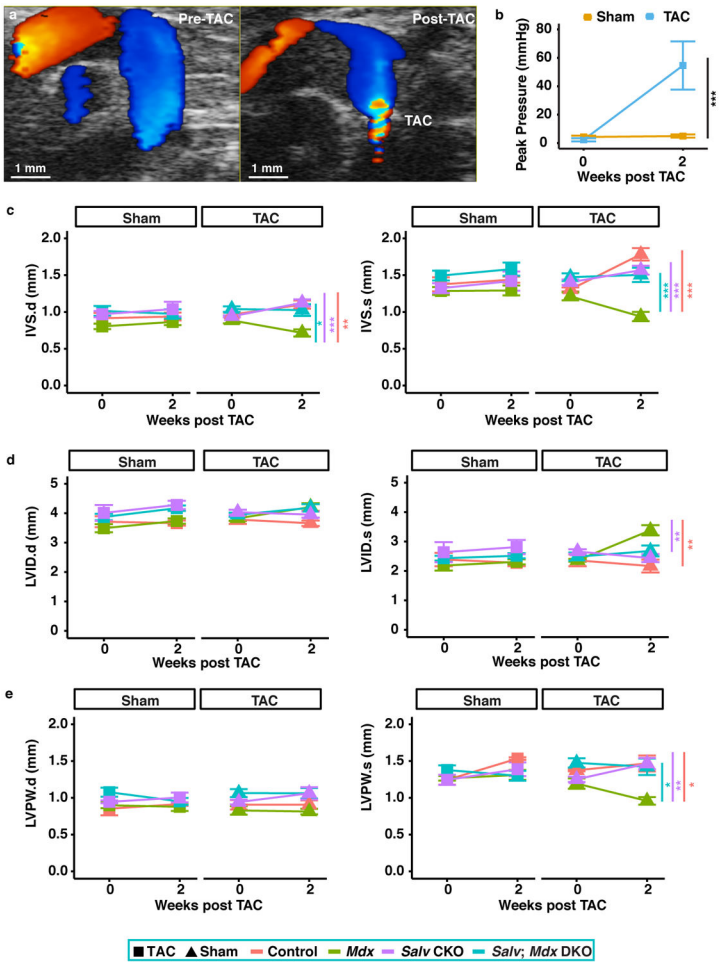

Extended Data Figure 4. Echocardiographic measurements

a, Color Doppler echocardiography across the transverse aorta before transverse aortic constriction (pre-TAC, left panel), and after transverse aortic constriction (post-TAC, right panel). The constriction site (TAC) is labeled on the post-TAC image. **b,** Doppler echocardiography measurement of peak pressure through the constriction site two weeks after TAC. Sham (n=9), TAC (n=7). Groups were compared by using analysis of variance (ANOVA) with the Tukey post-hoc test for pairwise comparisons, ***p<0.001. **c,** Interventricular septal (IVS) thickness during diastole (IVS.d, left panel) and systole (IVS.s, right panel). **d,** Left ventricular internal diameter (LVID) during diastole (LVID.d, left panel) and systole (LVID.s, right panel). **e,** Left ventricular posterior wall (LVPW) thickness during diastole (LVPW.d, left panel) and systole (LVPW.s, right panel). Sham control (n= 4); sham *Salv* conditional knockout (CKO, n=4); sham *Mdx* (n=6); sham *Salv*;*Mdx* double knockout (DKO, n=12). TAC control (n=5); TAC *Salv* CKO (n=8); TAC *Mdx* (n=5); TAC *Salv*;*Mdx* DKO (n=11). Groups were compared by using analysis of variance (ANOVA) with the Tukey post-hoc test for pairwise comparisons. Significant differences with the *Mdx* group two weeks post TAC are indicated. *p<0.05, **p<0.01, ***p<0.001.

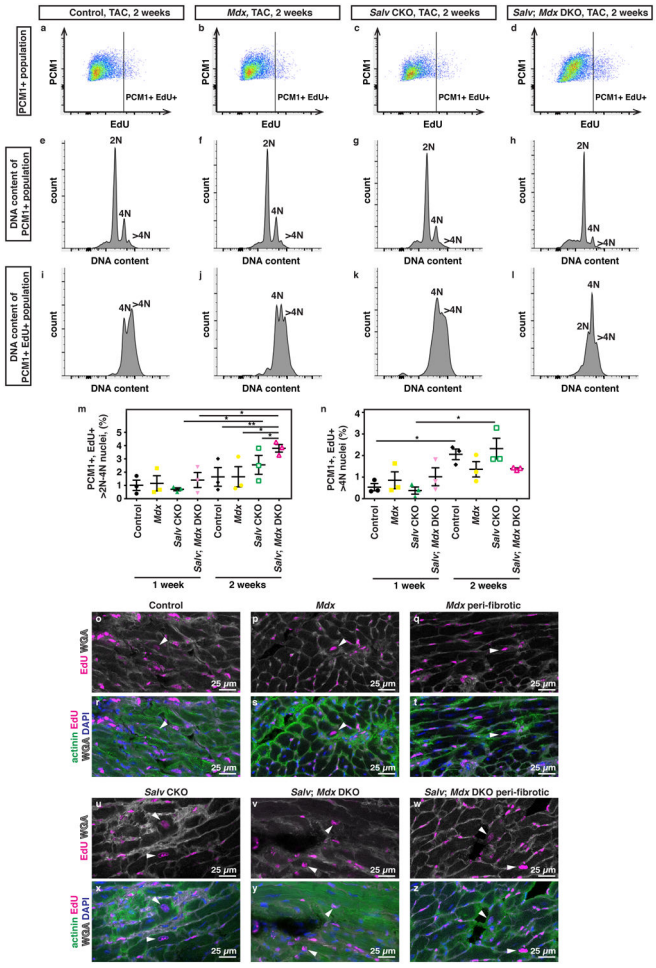

Extended Data Fig. 5. EdU incorporation analysis after transverse aortic constriction (TAC) surgery

a-n, Flow cytometry analysis on isolated nuclei after transverse aortic constriction (TAC) surgery. **a-l**, Representative images of flow cytometry analysis on the nuclei isolated from control (**a, e, i**), *Mdx* (**b, f, j**), *Salv* conditional knockout (CKO; **c, g, k**), and *Salv*;*Mdx* double knockout (DKO; **d, h, l**) mouse hearts after TAC surgery. **a-d,** PCM1+ population was gated and plots show EdU incorporation. **e-h**, Histogram showing DAPI intensity in PCM1+ population and discrimination between 2N, 4N, and >4N population. **i-l**, Histogram showing DAPI intensity in PCM1+, EdU+ population. **m, n**, Quantification of PCM1+, EdU + nuclei in >2N-4N (m) and >4N (n) population. Groups were compared by using analysis of variance (ANOVA) with the Tukey post-hoc test for pairwise comparisons (n=3). *p<0.05, **p<0.01. **o-v**, Representative images showing EdU staining of control (**o, u**), *Mdx* (**p, v**), peri-fibrotic area of *Mdx* (**q, w**), *Salv* conditional knockout (CKO) (**r, x**), *Salv*;*Mdx* double knockout (DKO; **s, y**) and peri-fibrotic area of DKO (**t, z**) mouse heart sections after TAC surgery collected after 2 weeks. CMs were stained for actinin and cells were delineated by WGA. Arrowheads show EdU-positive CMs. Quantification of EdU-positive CMs is shown in Figure 3n. Peri-fibrotic area defined in Methods.

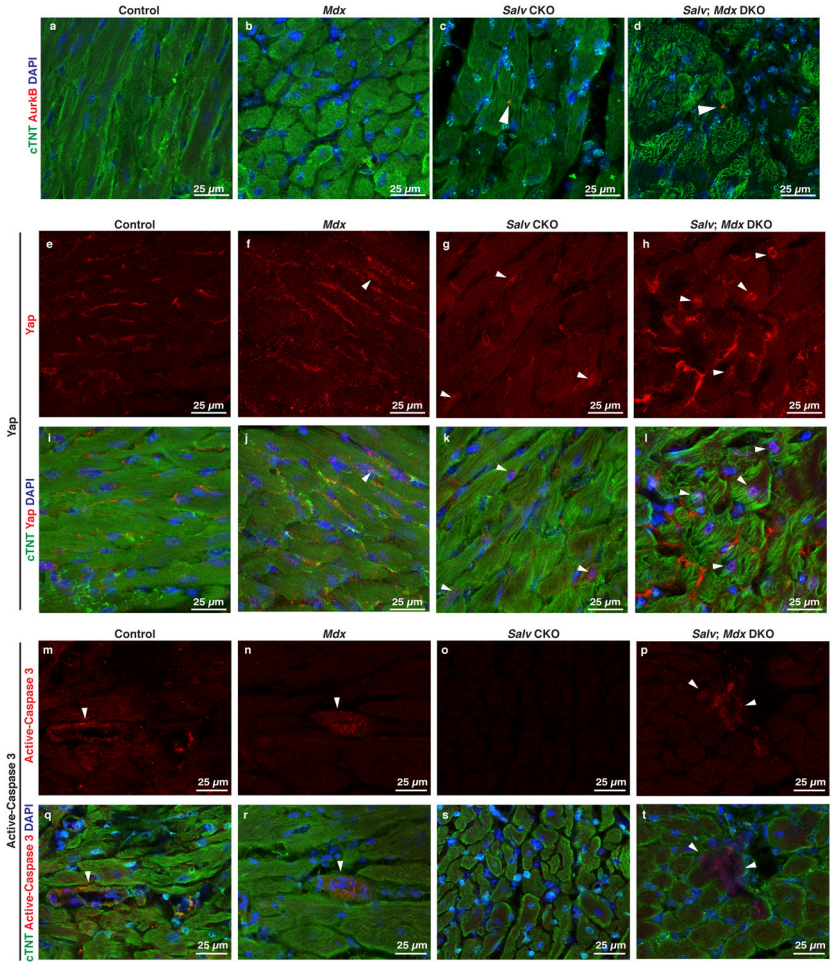

Extended Data Figure 6. Immunohistochemical analysis of mouse hearts after transverse aortic constriction (TAC) surgery

a-d, Representative images for aurora kinase B (AurkB) staining of control (**a**), *Mdx* (**b**), *Salv* CKO (**c**), and *Salv*;*Mdx* DKO (**d**) mouse hearts 2 weeks after TAC surgery. CMs were stained with anti-cTNT antibody. Quantification of AurkB-positive CMs is shown in Figure 3o. Arrowheads indicate positive AurkB staining. **e-k**, Representative images showing Yap staining of control (**e, i**), *Mdx* (**f, j**), *Salv* conditional knockout (CKO) (**g, k**), and *Salv*;*Mdx* double knockout (DKO; **h, l**) mouse hearts after TAC surgery. CMs were detected by immunostaining for cardiac troponin T (cTNT). Arrowheads point to Yap localized in nuclei. Quantification of CMs with nuclear Yap is shown in Figure 3p. **m-t**, Representative images for active caspase 3 staining of control (**m, q**), *Mdx* (**n, r**), *Salv* conditional knockout (CKO;**o, s**), and *Salv*;*Mdx* double knockout (DKO;**p, t**) mouse hearts 1 and 2 weeks after TAC surgery. CMs were stained with anti-cardiac troponin T (cTNT) antibody. Arrowheads show active caspase 3–positive CMs. Quantification of active caspase 3–positiveCMs is shown in Figure 3q.

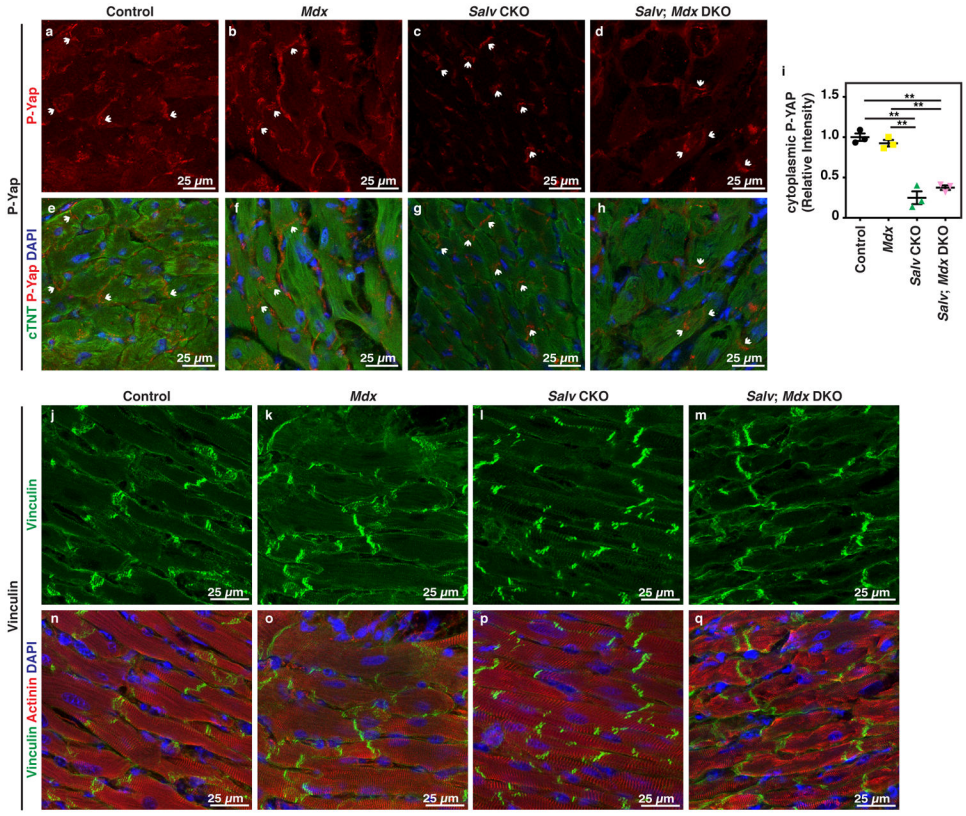

Extended Data Figure 7. Immunohistochemical analysis for phospho-Yap and Vinculin after transverse aortic constriction (TAC) surgery

a-h, Representative images showing phospho-Yap (P-Yap) staining of control (**a, e**), *Mdx* (**b, f**), *Salv* CKO (**c, g**), and *Salv*;*Mdx* DKO (**d, h**) mouse hearts after TAC surgery. CMs were detected by immunostaining for cardiac troponin T (cTNT). Arrows indicate P-Yap in intercalated discs. **i**, Quantification of P-Yap levels (n=3 for each genotype) measured according to pixel intensity. Groups were compared by using one-way analysis of variance with the Tukey post-hoc test for pairwise comparisons. **p<0.01. **j-q**, Representative images for vinculin staining of control (**j, n**), *Mdx* (**k, o**), *Salv* CKO (**l, p**), and *Salv*;*Mdx* DKO (**m, q**) mouse hearts after TAC surgery. Vinculin staining was used to detect cytoskeletal rearrangements in CMs after TAC surgery. Sarcomeres were stained with anti-sarcomeric actinin.

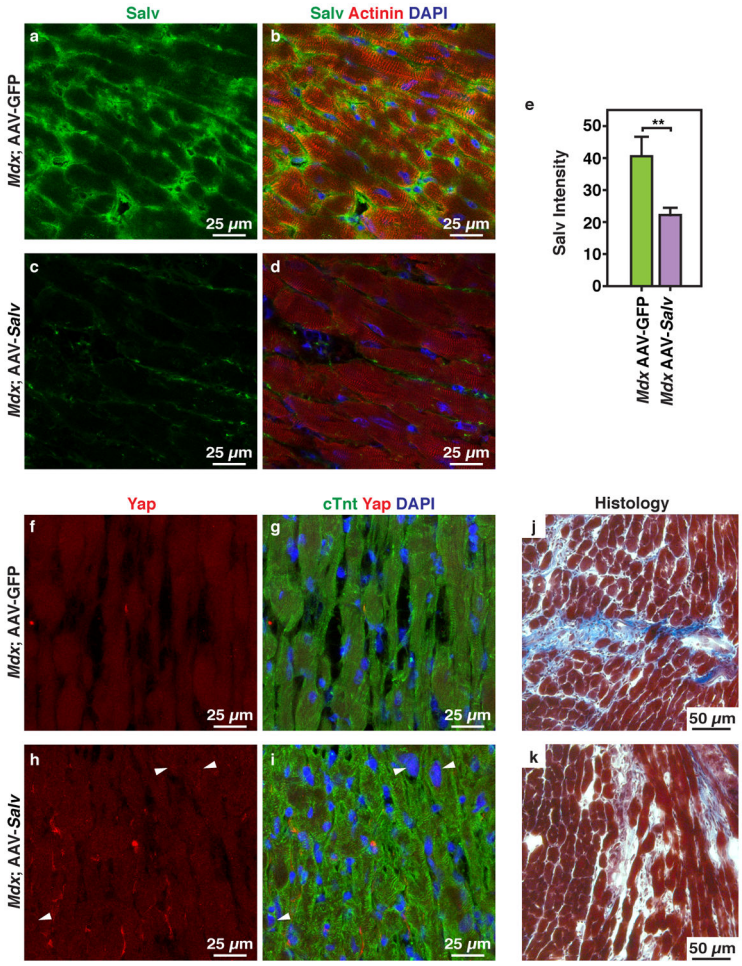

Extended Data Figure 8. Adeno-associated virus (AAV9)-treated *Mdx* hearts after transverse aortic constriction (TAC) surgery

Mouse hearts were collected 11 weeks after TAC surgery. **a-d**, Staining for Salvador in *Mdx* hearts transfected with AAV9-GFP (**a, b**) or AAV9-*Salv* (**c, d**). CMs were stained with actinin. **e**, Quantification of Salv (n=5 each treatment) measured according to pixel intensity. Groups were compared by using the Mann-Whitney U test. **p<0.01. **f-i**, Staining for Yap in *Mdx* mouse hearts transfected with AAV-GFP (**f, g)** or AAV-*Salv* (**h, i**). Arrowheads point to Yap localized in nuclei. **j, k**, Representative images showing trichrome staining of *Mdx* mouse hearts transfected with AAV9-GFP (**j**) or AAV9-*Salv* (**k**).

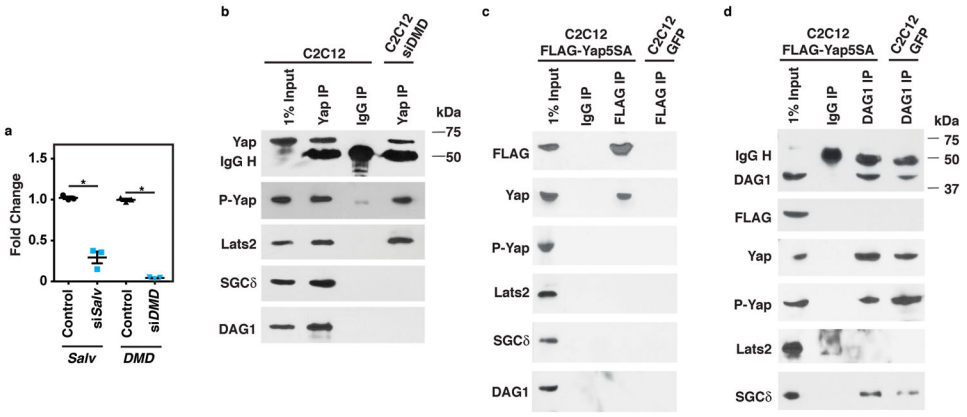

Extended Data Figure 9. Immunoprecipitation and subcellular localization studies in C2C12 cells

a, Knockdown efficiency of the small interfering (si)RNAs used in this study. C2C12 cells were differentiated and treated with si*Salv*, si*Dmd*, or control siRNA for 48 hours before harvesting. Groups were compared by using the Mann-Whitney U test (n=3 for each treatment). *p<0.05. **b-d**, Immunoprecipitation was performed by using protein extracts of differentiated C2C12 cells with antibodies specific for Yap (**b**), FLAG (c), or DAG1 (**d**), followed by immunoblotting of indicated proteins. Yap5SA or green fluorescent protein (GFP) constructs were transfected into C2C12 cells before differentiation (**c, d**). For gel source data, see Supplementary Figure 1.

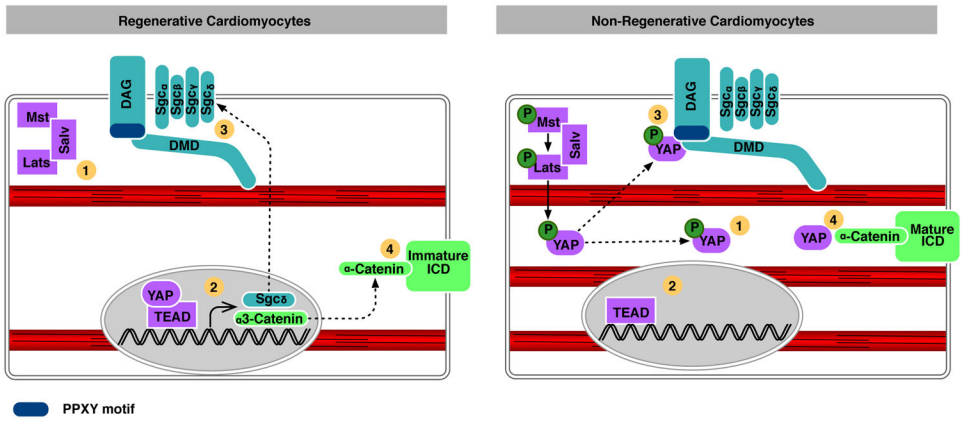

Extended Data Figure 10. Model of interaction between the Hippo pathway and the dystrophin glycoprotein complex (DGC)

ICD, intercalated disc.

(**Left side**)

1. Hippo signaling is low. YAP phosphorylation and YAP binding to the DGC is reduced.
2. YAP-TEAD promote the transcription of target genes including Sgcδ and α-catenin.
3. YAP-TEAD promote DGC assembly by promoting the expression of the core component Sgcδ.

4. The ICD is immature in neonatal cardiomyocytes. Yap promotes the expression of the ICD component α3-catenin.

(**Right side**)

1. Hippo signaling is high. YAP phosphorylation and YAP binding to the DGC is increased.
2. YAP-TEAD transcription-activating activity is reduced.
3. The DGC sequesters phosphorylated YAP through an interaction involving the PPxY motif of DAG1.
4. The ICD is mature in adult cardiomyocytes. YAP is incorporated into the ICD independent of Hippo through α-catenin binding.

Supplementary Material

Refer to Web version on PubMed Central for supplementary material.

Acknowledgments

This project was supported in part by an Intellectual and Developmental Disability Research Center grant (1U54 HD083092) from the Eunice Kennedy Shriver National Institute of Child Health & Human Development; the Mouse Phenotyping Core at Baylor College of Medicine with funding from the National Institutes of Health (U54 HG006348); and grants from the National Institutes of Health (DE 023177, HL 127717, HL 130804, and HL 118761 to J.F.M.) and the Vivian L. Smith Foundation (to J.F.M.). J.F.M. was supported by the Transatlantic Network of Excellence Award LeDucq Foundation Transatlantic Networks of Excellence in Cardiovascular Research 14CVD01: “Defining the genomic topology of atrial fibrillation.” T.H. was supported by the American Heart Association Scientist Development Grant (16SDG26460001). We thank Nicole Stancel, PhD, ELS, of the Texas Heart Institute, for editorial assistance.

References

1. Xin M, Olson EN, Bassel-Duby R. Mending broken hearts: cardiac development as a basis for adult heart regeneration and repair. Nature reviews Molecular cell biology. 2013; 14:529–541. DOI: 10.1038/nrm3619 [PubMed: 23839576]
2. Porrello ER, et al. Transient regenerative potential of the neonatal mouse heart. Science (New York, N Y). 2011; 331:1078–1080. DOI: 10.1126/science.1200708
3. Bergmann O, et al. Dynamics of Cell Generation and Turnover in the Human Heart. Cell. 2015; 161:1566–1575. DOI: 10.1016/j.cell.2015.05.026 [PubMed: 26073943]
4. Heallen T, et al. Hippo signaling impedes adult heart regeneration. Development. 2013; 140:4683–4690. [PubMed: 24255096]
5. Heallen T, et al. Hippo pathway inhibits Wnt signaling to restrain cardiomyocyte proliferation and heart size. Science (New York, N Y). 2011; 332:458–461. DOI: 10.1126/science.1199010
6. Morikawa Y, et al. Actin cytoskeletal remodeling with protrusion formation is essential for heart regeneration in Hippo-deficient mice. Sci Signal. 2015; 8:ra41. [PubMed: 25943351]
7. Ryder-Cook AS, et al. Localization of the mdx mutation within the mouse dystrophin gene. The EMBO journal. 1988; 7:3017–3021. [PubMed: 2903046]
8. Houtchens GR, Foster MD, Desai TA, Morgan EF, Wong JY. Combined effects of microtopography and cyclic strain on vascular smooth muscle cell orientation. Journal of biomechanics. 2008; 41:762–769. DOI: 10.1016/j.jbiomech.2007.11.027 [PubMed: 18222460]
9. van Westering TL, Betts CA, Wood MJ. Current understanding of molecular pathology and treatment of cardiomyopathy in duchenne muscular dystrophy. Molecules (Basel, Switzerland). 2015; 20:8823–8855. DOI: 10.3390/molecules20058823

10. Kassiri Z, et al. Combination of tumor necrosis factor-alpha ablation and matrix metalloproteinase inhibition prevents heart failure after pressure overload in tissue inhibitor of metalloproteinase-3 knock-out mice. Circulation research. 2005; 97:380–390. DOI: 10.1161/01.RES.0000178789.16929.cf [PubMed: 16037568]
11. Kamogawa Y, et al. Dystrophin-deficient myocardium is vulnerable to pressure overload in vivo. Cardiovasc Res. 2001; 50:509–515. [PubMed: 11376626]
12. Leach J, Martin JF. Hippo Pathway Deficiency Reverses Systolic Heart Failure. Preparation. 2016
13. Tommasi di Vignano A, Di Zenzo G, Sudol M, Cesareni G, Dente L. Contribution of the different modules in the utrophin carboxy-terminal region to the formation and regulation of the DAP complex. FEBS letters. 2000; 471:229–234. [PubMed: 10767429]
14. Zhao B, Li L, Tumaneng K, Wang CY, Guan KL. A coordinated phosphorylation by Lats and CK1 regulates YAP stability through SCF (beta-TRCP). Genes & development. 2010; 24:72–85. DOI: 10.1101/gad.1843810 [PubMed: 20048001]
15. Li J, et al. Alpha-catenins control cardiomyocyte proliferation by regulating Yap activity. Circulation research. 2015; 116:70–79. DOI: 10.1161/circresaha.116.304472 [PubMed: 25305307]
16. Halder G, Dupont S, Piccolo S. Transduction of mechanical and cytoskeletal cues by YAP and TAZ. Nature reviews Molecular cell biology. 2012; 13:591–600. DOI: 10.1038/nrm3416
17. Long C, et al. Postnatal genome editing partially restores dystrophin expression in a mouse model of muscular dystrophy. Science (New York, N Y). 2016; 351:400–403. DOI: 10.1126/science.aad5725
18. Nelson CE, et al. In vivo genome editing improves muscle function in a mouse model of Duchenne muscular dystrophy. Science (New York, N Y). 2016; 351:403–407. DOI: 10.1126/science.aad5143
19. Tabebordbar M, et al. In vivo gene editing in dystrophic mouse muscle and muscle stem cells. Science (New York, N Y). 2016; 351:407–411. DOI: 10.1126/science.aad5177
20. McGreevy JW, Hakim CH, McIntosh MA, Duan D. Animal models of Duchenne muscular dystrophy: from basic mechanisms to gene therapy. Dis Model Mech. 2015; 8:195–213. DOI: 10.1242/dmm.018424 [PubMed: 25740330]
21. Alkass K, et al. No Evidence for Cardiomyocyte Number Expansion in Preadolescent Mice. Cell. 2015; 163:1026–1036. DOI: 10.1016/j.cell.2015.10.035 [PubMed: 26544945]
22. Richardson GD. Simultaneous Assessment of Cardiomyocyte DNA Synthesis and Ploidy: A Method to Assist Quantification of Cardiomyocyte Regeneration and Turnover. Journal of visualized experiments: JoVE. 2016

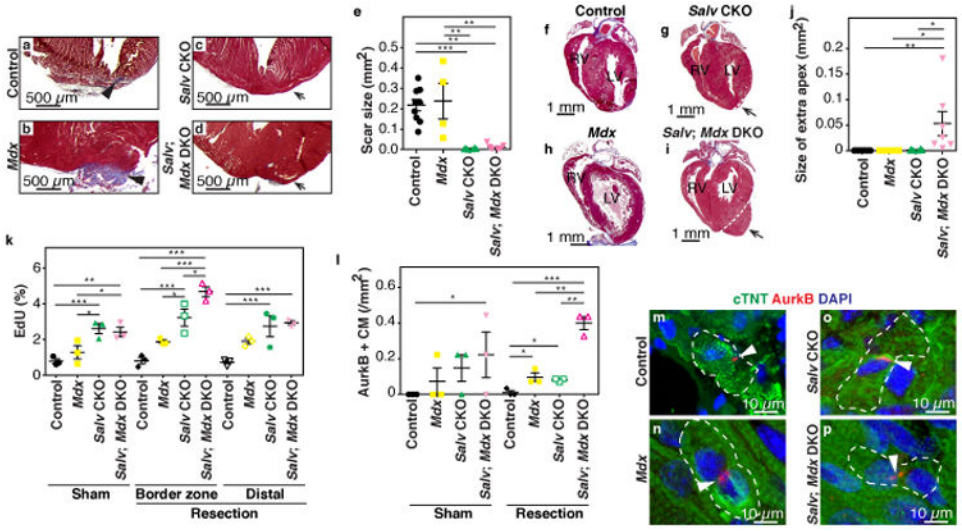

Figure 1. Combined loss of the dystrophin glycoprotein complex and Hippo pathway in the injured heart

a-d, Trichrome-stained sections of heart apex 21 days after resection. Fibrotic scar (arrowheads) and extra apex (arrows) are denoted. **e**, Fibrotic scar quantification: control (n=9), *Mdx* (n=4), *Salv* CKO (n=6), and *Salv;Mdx* DKO (n=7). Comparisons by analysis of variance (ANOVA) with Bonferroni's multiple comparison test for pairwise comparisons. **p<0.01, ***p<0.001. **f-i**, Sections showing extra apex (arrows). Dotted lines show resection plane. LV, left ventricle, RV, right ventricle. **j**, Quantification of extra apex size: control (n=9), *Mdx* (n=4), *Salv* CKO (n=6), and *Salv;Mdx* DKO (n=7). Comparisons by ANOVA with Bonferroni's multiple comparison test for pairwise comparisons. *p<0.05, **p<0.01. **k**, Quantification of EdU-positive CMs (n=3 for each). EdU was injected 4 hours before collection. Comparisons by ANOVA with Bonferroni's post-hoc test for pairwise comparisons. *p<0.05, **p<0.01, ***p<0.001. **l**, Quantification of AurkB-positive CMs (n=3 for each). Comparisons by ANOVA with the Mann-Whitney test for pairwise comparisons. *p<0.05, **p<0.01, ***p<0.001. **m-p**, Immunohistochemical staining of AurkB-positive CMs (arrowheads) Dotted lines delineate dividing CMs. CMs were stained for cardiac troponin T (cTNT), and nuclei with DAPI.

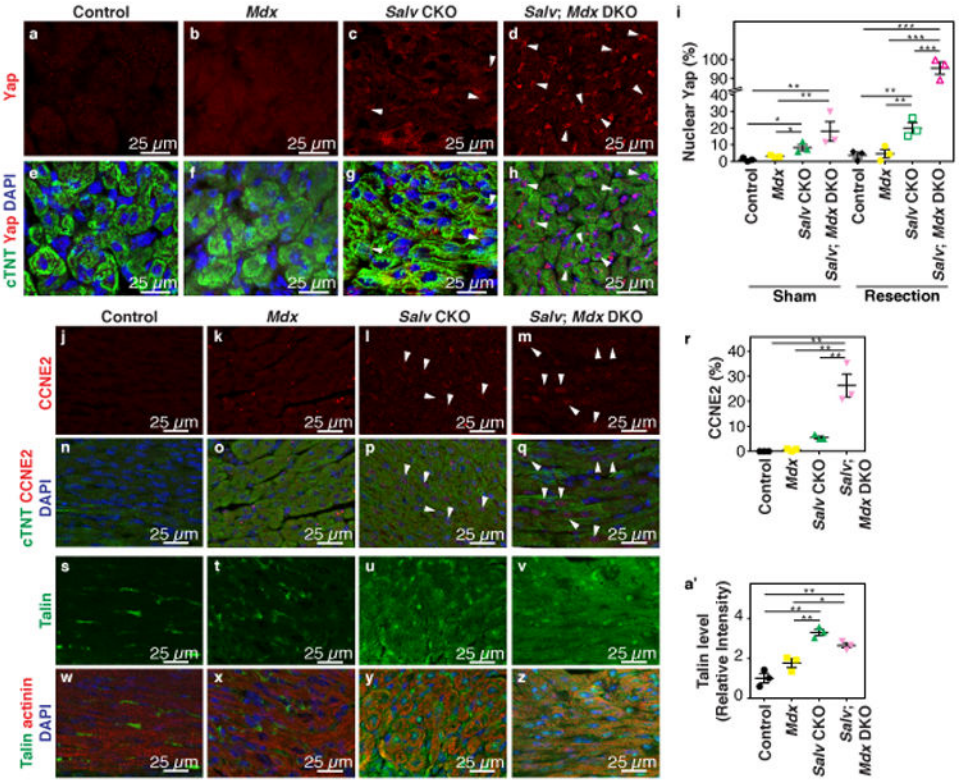

Figure 2. Yap subcellular localization and expression of downstream targets in Hippo-deficient *Mdx* cardiomyocytes after apex resection

a-i, Immunohistochemical staining showing Yap localization 4 days after apex resection. CMs were stained cTNT and nuclei with DAPI. Nuclear Yap (arrowheads). **i**, Nuclear Yap quantification in CMs (n=3 for each). Comparisons by two-way ANOVA with Mann-Whitney test for pairwise comparisons. *p<0.05, **p<0.01, ***p<0.001. **j-r**, Immunohistochemical staining of CCNE2 (arrowheads). **r**, Quantification of CCNE2-positive CMs (n=3 for each). Comparisons by one-way ANOVA with Tukey post-hoc test for pairwise comparisons. **p<0.01. **s-a′**, Talin immunohistochemical staining. CMs stained for sarcomeric actinin, and nuclei with DAPI. **a′**, Talin quantification (n=3 for each), measured by pixel intensity. Comparisons by one-way ANOVA with Tukey post-hoc test for pairwise comparisons. *p<0.05, **p<0.01.

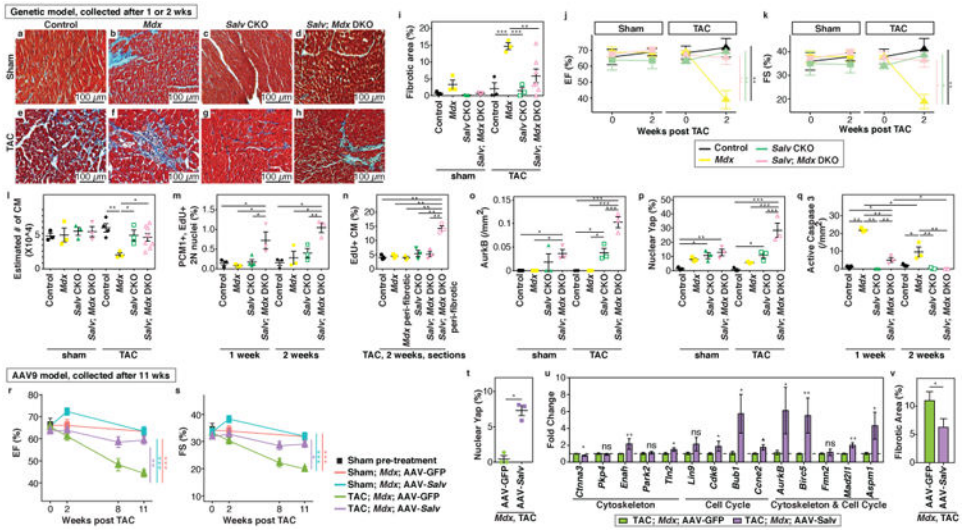

Figure 3. Suppression of *Mdx* cardiomyopathy by Hippo deletion in a pressure overload model

a-n, Transverse aortic constriction (TAC) or sham surgery in 9-week-old control (n=4 for sham, n=5 for TAC), *Mdx* (n=6 for sham, n=5 for TAC), *Salv* conditional knockout (CKO; n=4 for sham, n=8 for TAC), and *Salv*;*Mdx* double knockout (DKO; n=12 for sham, n=11 for TAC). **a-h**, Trichrome stained sections 2 weeks after sham (**a-d**) or TAC (**e-h**). **i**, Fibrotic area quantitation. Comparisons by analysis of variance (ANOVA) with Bonferroni's post-hoc test for pairwise comparisons (n=7 for DKO TAC group, n=3 for all others). **p<0.01, ***p<0.001. **j, k**, Ejection fraction (EF) and fractional shortening (FS). Detailed analyses are in Extended Data Fig. 4. Comparisons by ANOVA with Tukey post-hoc test for pairwise comparisons. *p<0.05, **p<0.01. **l**, Estimation of total CM number. Comparisons by ANOVA with Bonferroni's post-hoc test for pairwise comparisons (n=4 for control TAC group, n=8 for DKO TAC group, n=3 for others). *p<0.05, **p<0.01, ***p<0.001. **m**, EdU incorporation in diploid CM nuclei by flow cytometry after TAC. Representative images of flow cytometry are in Extended Data Fig. 5a-l. Comparisons by ANOVA with Tukey post-hoc test for pairwise comparisons (*Salv*CKO 1 week n=4; n=3 for all others). *p<0.05, **p<0.01. **n**, CM EdU incorporation using tissue sections. Representative images are in Extended Data Fig. 5o-z. Comparisons by ANOVA with Tukey post-hoc test for pairwise comparisons (n=3 for each). **p<0.01. **o**, Quantification of AurkB positive CMs. Representative images are in Extended Data Fig. 6a-d. Comparisons by ANOVA with Bonferroni's post-hoc test for pairwise comparisons (n=3 for each). *p<0.05, *** p<0.001. **p**, Quantification of nuclear localized Yap in CMs. Representative images are in Extended Data Fig. 6e-l. Groups compared by ANOVA with Bonferroni's post-hoc test for pairwise comparisons (n=3 for each). *p<0.05, **p<0.01, ***p<0.001. **q**, Active caspase 3–positive CMs quantification at 1 week and 2 weeks after TAC. Representative images are in Extended Data Fig. 6m-t. Comparisons by one-way analysis of variance with Tukey post-hoc test for pairwise comparisons (n=3 for each). *p<0.05, **p<0.01. **r, s**, EF and FS in TAC (n=10 for AAV-GFP, n=9 for AAV-*Salv*) and sham (n=8 for AAV-GFP, n=10 for AAV-*Salv*). Week 11 comparisons by ANOVA with Tukey post-hoc test for pairwise comparisons. *p<0.05, **p<0.01, ***p<0.001. **t**, Nuclear Yap quantification in CMs. Comparisons by Mann-Whitney U test (n=3 for each). *p<0.05. Representative images in Extended Data Fig.

8f-i. **u**, QRT-PCR of Yap target genes. Comparisons by Mann-Whitney U test (n=5 for each treatment). *p<0.05, **p<0.01. ns, nonsignificant. **v**, Fibrotic area quantification. Comparisons by Mann-Whitney U test (n=5 for each treatment). Representative images in Extended Data Fig. 8j, k.

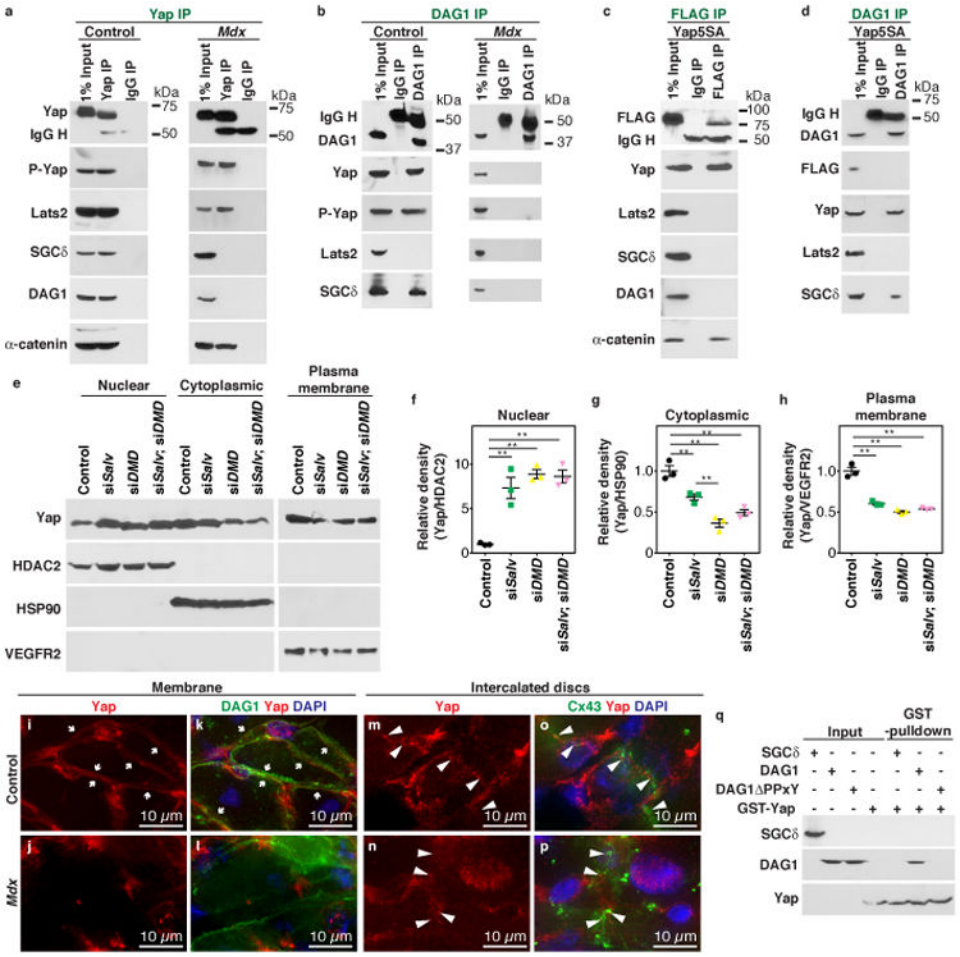

Figure 4. Yap binding to the dystrophin glycoprotein complex

a, b, Immunoprecipitation (IP) of P12 control and *Mdx* mouse hearts for Yap (**a**) or DAG1 (**b**), with immunoblotting of indicated proteins (n=3 for each). **c, d**, IPfor FLAG(c) and DAG1 (**d**) from 6-week-old Yap5SA-expressing hearts with immunoblotting of indicated proteins (n=3 each). **e-h**, YAP subcellular localization C2C12 cells. Comparisons by ANOVA with Tukey post-hoc test for pairwise comparisons (n=3 for each). **p<0.01. **i-p**, Deconvolution epifluorescence (super-resolution) microscopic images of Yap subcellular localization in 11-week-old hearts; Cx43, Connexin 43. Yap localization in membrane (arrows) and intercalated discs (arrowhead). **q**, GST fusion protein binding assay for indicated proteins. DAG1ΔPPxY, DAG1 PPxY motif deletion. Gel source data (Supplementary Figure 1).